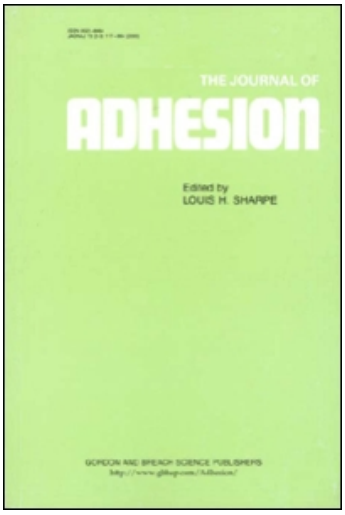

The Journal of Adhesion

Publication details, including instructions for authors and subscription information:
http://www.informaworld.com/smpp/title~content=t713453635

Determining the Effective Material Properties of Damaged Particle-Filled Adhesives

I. N. Bysh[a]; A. D. Crocombe[a]; P. A. Smith[b]
[a] Department of Mechanical Engineering, University of Surrey, Guildford, UK [b] Department of Materials Science and Engineering, University of Surrey, Guildford, UK

To cite this Article Bysh, I. N. , Crocombe, A. D. and Smith, P. A.(1996) 'Determining the Effective Material Properties of Damaged Particle-Filled Adhesives', The Journal of Adhesion, 58: 3, 205 — 226
To link to this Article: DOI: 10.1080/00218469608015201
URL: http://dx.doi.org/10.1080/00218469608015201

J. Adhesion, 1996, Vol. 58, pp. 205–226
Reprints available directly from the publisher
Photocopying permitted by license only

Determining the Effective Material Properties of Damaged Particle-Filled Adhesives*

I. N. BYSH, A. D. CROCOMBE**

Department of Mechanical Engineering, University of Surrey, Guildford, GU2 5XH, UK

P. A. SMITH

Department of Materials Science and Engineering, University of Surrey, Guildford, GU2 5XH, UK

(Received March 28, 1995; in final form September 1, 1995)

The damage occurring on the micro-structural level in a commercially available filled epoxy adhesive has been investigated. Scanning electron microscopy of loaded bulk compact tension specimens has provided quantitative data regarding the size and distribution of the damage, which, for the particular adhesive under investigation, takes the form of particle cracking and debonding. Finite element analyses were carried out on representative unit cells of the material. These provided properties for the base epoxy adhesive which were used to determine the macroscopic elastic constants of the damaged material. These macroscopic properties can be used in further analyses to assess the effect that the presence of damaged material has on a system.

KEY WORDS: Adhesive microstructure; unit cell; particle debonding; microstructural damage; macroscopic material properties; particle filled adhesives.

1. INTRODUCTION

Epoxy resins are the basis of many modern structural adhesives[1]. Neat epoxy needs toughening, so another phase of rubber is often added. Unfortunately, rubber causes a significant reduction in stiffness, so the adhesive is filled with a rigid phase[2]. Manufacturers have found that certain combinations of rubber and filler are better tougheners than others. Much research has been carried out to identify and model toughening mechanisms, notably by Kinloch *et al.*[2,3] and Pearson *et al*[4,5]. This paper presents experimental investigations of damage, and associated mechanical modelling in a widely available commercial adhesive system, comprising an epoxy resin filled with an inorganic second phase.

From an engineering point of view, understanding the toughening mechanisms is incidental if no way can be found to predict the failure conditions in an adhesive joint. A

* Presented at EURADH94, Mulhouse, France, September 12–15, 1994, a conference organized by the Section Française de l'Adhesion, division de la Société Française du Vide.

** Corresponding author.

finite element approach is attractive, because geometries may be modelled that have either no, or a very complex, analytical solution. However the damaged adhesive material properties must still be found since a loaded joint contains regions with such material. Einstein[6] in 1906 first investigated the effective material properties of particulate composites by calculating the effective viscosity of a fluid containing rigid spherical particles. It was not until 1963 that Hill[7] and Hashin[8] deduced elastic moduli by making use of the fundamental postulate of elastic heterogeneous media states, later defined by Hashin[9] as "the stress and strain fields in a large heterogeneous body that is statistically homogeneous subjected to homogeneous boundary conditions are statistically homogeneous, except in a boundary layer near the external surface." "Statistically homogenous" is not the same as being structurally homogeneous; indeed, every material has an inhomogeneous microstructure, a fact that conventional elastic theory ignores. When the microscopic elements of a material become too disimilar, predicting the macroscopic material properties becomes complicated, and principles such as statistical isotropy have to be invoked. Simply speaking, a statistically-isotropic process has statistical properties (such as average nearest neighbour distance) that are independent of sample orientation or location. Ripley[10] provides a good introduction to this and to the concept of structural homogeneity.

There have been three main ways in which statistically-isotropic materials have been analysed to predict their material properties. The direct approach[7,11] attempts to express the effective moduli in terms of the individual moduli of the constituent materials. It really only has any value for the case of an isolated particle, or for special cases of finite particle concentrations, for instance weakly inhomogenous systems where the local moduli vary by only a small amount from their average value. Hashin[11] modelled a composite sphere assemblage, but only obtained the bulk modulus. Similarly, Hill[7] could find the bulk modulus for an arbitrary phase geometry, but only for materials whose shear moduli were equal.

The second approach-variational bounding- is so-called because it identifies higher and lower bounds for the shear and bulk moduli, usually from consideration of the expressions for strain energy and stress energy. If high order statistical information is available (*i.e.*, the variation of the polarisation tensor), really quite close bounds may be described (Hashin and Shtrikman[12]), but once the ratio of the individual elastic moduli exceeds about 10, the analysis is no longer strictly valid. Thus, it cannot be used to model holes or rigid particles. Close bounds may also be derived for a particular statistical model as long as the limited applicability can be tolerated. For instance, Hashin[11,13,14] used the technique to model the composite sphere assemblage by considering the minimum potential and complementary energies.

The third, and most popular, approach uses a concept known as the self-consistent scheme. A particle is considered to be embedded in a homogeneous material with material properties equal to the (as yet unknown) effective macroscopic material properties. It is treated as a boundary value problem, with the particle strain being expressed in terms of the effective macroscopic bulk and shear moduli. The embedded particle may be ellipsoid (Eshelby[15] and Wu[16]) or spherical (Budiansky[17] and Hill[18]). The problem with the self-consistent scheme is that it takes the particle out of context. It assumes the particle sees a homogenous matrix and is unaffected by the stress interactions from the surrounding particle array. In other words, the particle by itself is not representative of a typical, statistically-isotropic volume of material. A method that

circumvents this problem to a certain extent, known as the generalised self-consistent scheme, has the particle embedded in a matrix shell, which in turn is embedded in the homogeneous material with unknown macroscopic effective properties. This added degree of complexity gives a result that can only be evaluated numerically, but Kerner[19] first gave results for effective bulk modulus, followed by Smith[20] and Christiansen and Lo[21] with an effective bulk shear modulus.

As far as damaged material is concerned, the self-consistent method has been used to determine the effective properties for material containing an array of cracks. Once again, there is a distinction made between the self-consistent method, which considers a crack embedded directly in a material of unknown elastic properties[22–25], and the generalised self-consistent method, which takes the crack to be embedded in a matrix which, in turn, is embedded in the medium of unknown properties[19,21,26,27]. Nonlinear simultaneous equations for the overall material constants may either be obtained from considering the jumps of displacement across the crack and the discontinuity of the displacement field, or the energy of the cracked medium only and the energy of the crack, the inclusion and the effective medium. Aboudi and Benveniste[26] solved the problem for a randomly orientated and distributed array of microcracks. Other models have been developed to include anisotropy: Gottesman, Hashin and Brull[28] use the self-consistent method to predict the effect of a perfectly-aligned array of microcracks on the moduli of an anisotropic material; Horii and Nemat-Nasser[25] consider a randomly orientated distribution of microcracks and include the effects of crack face friction in the model. Since the frictional effects can produce directional properties, load-induced anisotropy may be predicted. A problem with these models is that they are only valid for low volume fractions. Santare *et al.*[27] considered an elliptical, as opposed to a spherical, inclusion, and managed to obtain accurate results even for high volume fractions of inclusions.

An alternative approach to modelling the effective material properties is to use a finite element analysis. The method used here to model the adhesive is based on the concept of a unit cell. Davy and Guild[29] presented a statistical justification of this method. The filler is assumed to be uniformly distributed in three dimensions throughout the adhesive, and a Gibbs hard core process[10] is used to determine the expected dimensions of a single particle surrounded by matrix. The shape of the cell and particle is arbitrary but, for this paper, a circular particle in a square cell and a spherical particle in a cylindrical cell are considered. Analysing the unit cell is equivalent to analysing the composite material as a whole.

The finite element approach has been used in preference to the other closed form approaches for several reasons:

- The development of an alternative to analyses such as the generalised self-consistent scheme is in general beneficial, since one may be used to verify the other.
- The unit cell may be used to develop failure criteria as well as to provide effective material properties.
- The finite element philosophy is more readily understood.
- The finite element unit cell may be easily adapted to model damaged morphologies that are not amenable to the techniques discussed above.

A problem with using a commercial adhesive is the reticence on the part of the manufacturers to reveal the exact nature of the material's component parts. The unit

cell approach was, therefore, also used to determine the elastic properties of the two phases from a knowledge of the composite material behaviour.

The structure of the present paper is as follows: The first two sections describe briefly how the microscopic composition of the adhesive was determined, and how damage was seen to propagate within it. In sections 4 and 5, this information is used in a finite element unit cell analysis to deduce the elastic properties of adhesive containing damage. Section 4 discusses the theory for the unit cell and presents a validation of the technique using three data sets for particle-filled matrices from the literature. In section 5, the unit cell is used to calculate the material properties of the adhesive's constituent parts, and to calculate the material properties of damaged adhesive.

2. DETERMINATION OF MORPHOLOGY

In the system under investigation, rigid inorganic filler is present in powdered form. In order to analyse the damage, it was necessary to determine the volume fraction and average filler particle size and shape from scanning electron microscope (SEM) photomicrographs of polished samples (see Fig. 1). Photographs of the adhesive were digitised using an Epson GT-8000 scanner, and image processed to locate, count and measure the particles. The size of the particles was calculated by drawing a best fit ellipse through the particle boundary and finding the major and minor axis lengths. The particle area fraction was found by dividing the total area of cross-sectioned

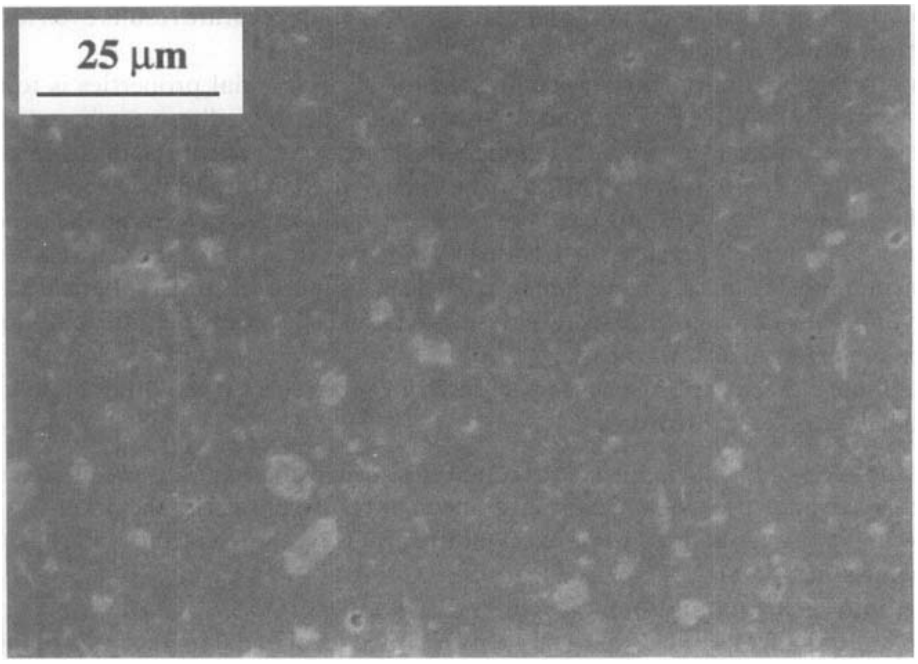

FIGURE 1 An SEM photomicrograph showing the surface of polished two-phase adhesive. The calculated volume fraction was 12%.

particles by the overall micrograph area. Assuming randomly distributed particles, the volume fraction can be set equal to the area fraction.

3. DAMAGE OBSERVED IN COMPACT TENSION TESTS

Compact tension specimens of bulk adhesive, 6 mm (thickness) × 24 mm × 25 mm, were tested using either an Instron 6025 tensile testing machine or a special straining stage designed to fit within the vacuum chamber of an SEM. In each case, the damage observed in the specimens prior to catastrophic failure was similar. The main crack is banded on each side by a damaged region of size approximately 30 μm. Apart from the main crack, the epoxy in the damaged region shows no sign of cracking, and the only micro-cracking present is associated with the filler particles. They have either fractured throuth their bulk or debonded. The in-situ SEM tests showed that cracking and debonding of the particles preceded the main crack growth which proceeds by the linkage of these defects. Figure 2 shows a photomicrograph of a compact tension specimen through which a crack has propagated, leaving damage in its wake. Ellis *et al.*[30] noticed a similar phenomenon in an epoxy adhesive filled with calcium silicate. In order to understand the effect of the filler particle cracking on the macroscopic material behaviour near the main crack tip, finite element analyses have been used to determine appropriate reduced elastic properties for the adhesive.

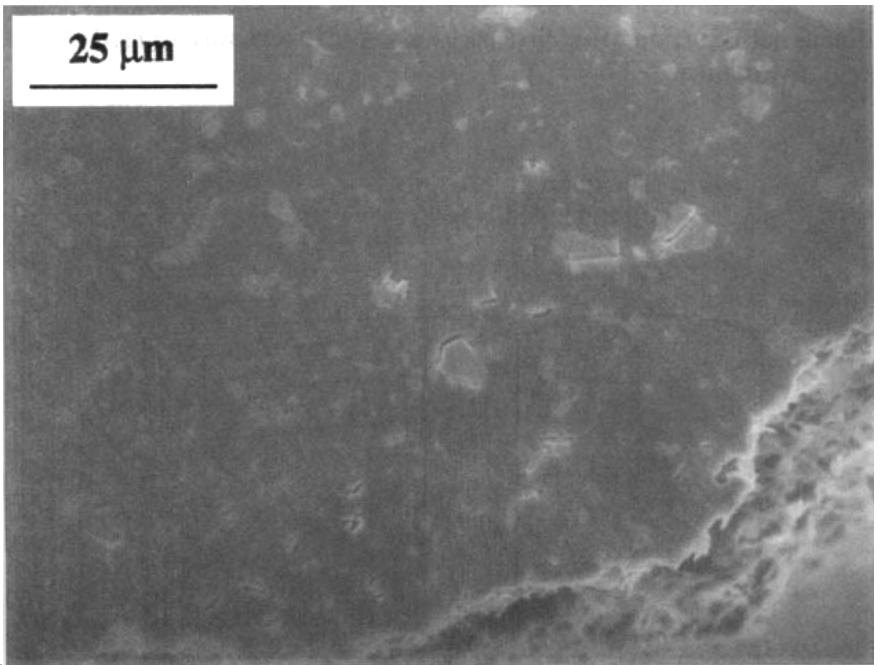

FIGURE 2 An SEM photomicrograph showing damage on the surface of a polished compact tension specimen of the adhesive. Note the extent of the damaged zone and the two types of filler particle failure-debonding and cracking.

4. EFFECTIVE ELASTIC MATERIAL PROPERTIES OF PARTICULATE SYSTEMS

4.1 Introduction

Bulk tensile tests using dog-bone samples[31] indicate that the adhesive has an elastic modulus of 3265 MPa, and a Poisson's ratio of 0.406. These, of course, are composite values, and if the system is to be modelled on a microscopic level, then the material properties of the system components must be determined. To this end, it was decided to model a unit cell of matrix containing a filler particle. The problem in doing this was to find a cell representative of the real case. Davy and Guild[29] modelled the experimental data of Smith [32] for the elastic properties of epoxy filled with varying volume fractions of glass beads. They present a sophisticated statistical method to determine the dimensions of a particular unit cell shape, based on interparticle distance, and obtained very good predictions of the data.

Any shape may be chosen for the unit cell. Every shape has a typical interparticle distance, and this must be equated to the expected interparticle distance of the filler dispersion. The expected distance is derived from consideration of the Voronoi tessellation of a random three-dimensional distribution of points. Because the particles have a finite radius, a hard-core Gibbs process is used to derive the actual interparticle distance distribution. In fact, the cell chosen by Davy and Guild was a spherical particle within a cylinder, as in Figure 3. The theory works just as well in two dimensions, however, and the cell chosen for the remainder of this work was a circular particle within a square. The finite element model is identical to that shown in Figure 3, the only difference being that two-dimensional plane elements are employed instead of axisymmetric elements. In order to assess how closely the unit cell approach simulates the actual material behaviour, it is first necessary to devise a way to load the cell in a representative manner.

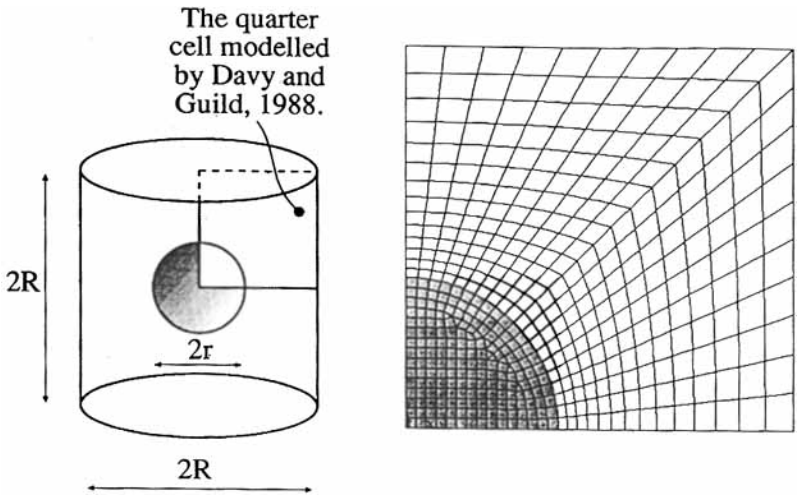

FIGURE 3 The axisymmetric cell used by Davy and Guild, showing within it the quarter cell that may be used in an axisymmetric finite element analysis.

4.2 Boundary Conditions

Davy and Guild[29] loaded their cylinder by applying a known strain in the axial (vertical) direction, whilst constraining all the nodes on the vertical faces to move horizontally by an equal distance (Fig. 4a). These boundary conditions imitate the effect on the cell of the surrounding material. The elastic modulus is calculated by dividing the resulting average axial stress by the applied axial strain. This operation is only acceptable because the hoop and radial stresses average to zero.

The drawback to the cylindrical unit cell is that it does not behave in an isotropic manner. This makes it impossible to determine a shear modulus and difficult to interpret the directional properties of the cell. A two-dimensional square cell, on the other hand, although not being isotropic either, can be loaded in mutually perpendicular directions and also in shear. Thus, shear as well as direct moduli may be calculated, and by applying suitable multiples of unit strains, directional loading may be simulated. Unfortunately loading the cell in this way constrains the boundaries to deform in straight lines, something that does not happen in the bulk. Some way must be found to load the cell whilst allowing the boundaries to assume an appropriate shape.

One approach is to require that each cell must remain fully compatible with its adjacent cells. In other words, the deformed cells must fit together perfectly. Although there exists an infinite number of possible unit cells, a square cell is obviously the most convenient on which to impose the necessary boundary conditions. This approach is different from that of Davy and Guild who assume a property function that relates the applied load to the required material property (stiffness or Poisson's ratio).

With reference to Figure 4, a point, e, on the left hand side boundary of the cell has horizontal and vertical displacements u_e and v_e, respectively, and a corresponding point, g, on the right hand side has displacements u_g and v_g. The cell is subjected to strains in the horizontal and vertical directions, and shear strain as indicated in Figure

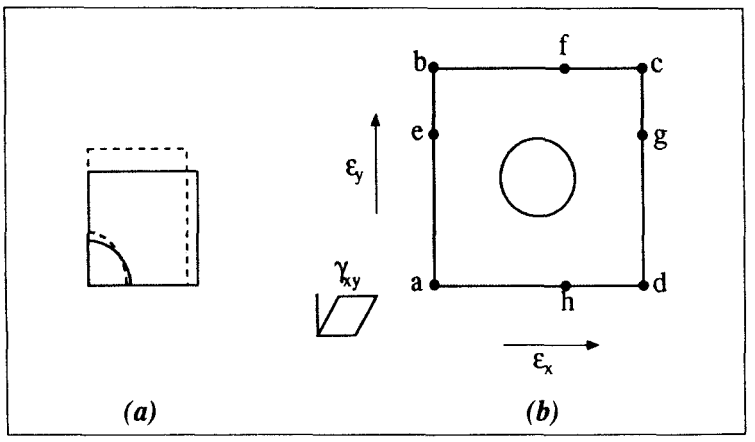

FIGURE 4 The different loading regimes adopted by a) Davy and Guild; b) The present authors.

4. The boundary conditions applied to the vertical sides can be written:

$$u_g - u_e = a\varepsilon_x \tag{1}$$

$$v_g - v_e = a\gamma_{xy} \tag{2}$$

where a = side of cell
ε_x = strain in the horizontal direction
γ_{xy} = shear strain

Similar conditions are applied to the horizontal boundaries, this time employing the vertical linear strain.

4.3 Validation of the Unit Cell Technique

Three different data sets were chosen:

i) Smith[32] presented experimental results for the variation of modulus and Poisson's ratio of epoxy filled with glass spheres as a function of filler volume fraction. This data set has been modelled using both the axisymmetric approach of Davy and Guild, and the two-dimensional circle-in-square approach.
ii) Pearson and Yee[33] provide data for the variation of modulus with volume fraction for rubber spheres in epoxy matrix. These results were modelled by Guild and Young[34] using the same cylindrical unit cell as Davy and Guild[29]. The trend is for decreasing stiffness with increasing volume fraction of rubber which is in contrast to the first data set and, obviously, models the behaviour of a traditionally toughened epoxy resin.
iii) Hasselmann and Fulrath[35] obtained similar stiffness *versus* volume fraction data for mica particles in glass. Their work was modelled by Agarwal *et al.*[36], again with the cylindrical unit cell.

The material properties used in these analyses are shown in Table I. Comparisons between these sets of experimental data and finite element models are shown in Figures 5 to 8. Perhaps the most illustrative data set is the first, since the elastic properties of its components are closest to those in the system presently under study. Davy and Guild achieve a better prediction of Smith's experimental results with their three-dimensional model, especially as the volume fraction rises above 15%. At low volume fractions, however, both models predict the actual system behaviour with reasonable accuracy.

TABLE I
Material properties used in the FE analyses

Data set	Matrix Material		Filler Material	
	Modulus [MPa]	Poisson's ratio	Modulus [MPa]	Poisson's ratio
Glass spheres in epoxy[32]	3010	0.394	76000	0.23
Rubber in epoxy[33]	3210	0.35	0.4	0.499
Mica in glass[35]	81360	0.197	416500	0.257

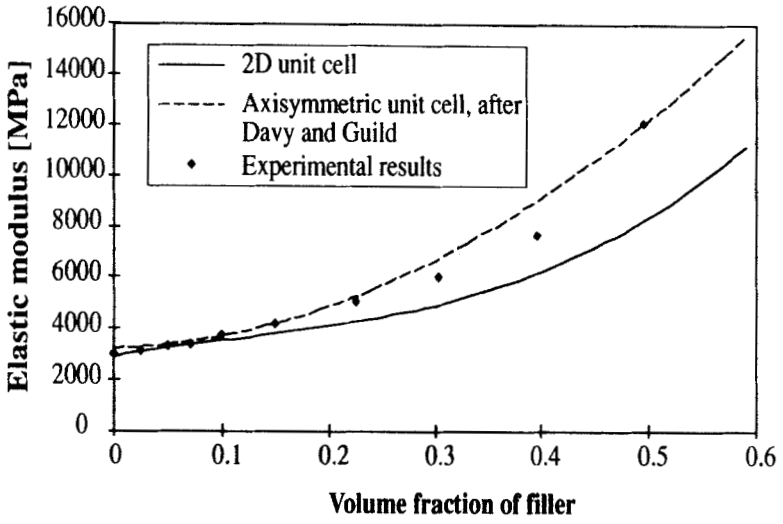

FIGURE 5 Elastic modulus as a function of volume fraction for data set i), *i.e.* glass spheres in epoxy. Finite element results for a two-dimensional unit cell and an axisymmetric unit cell.

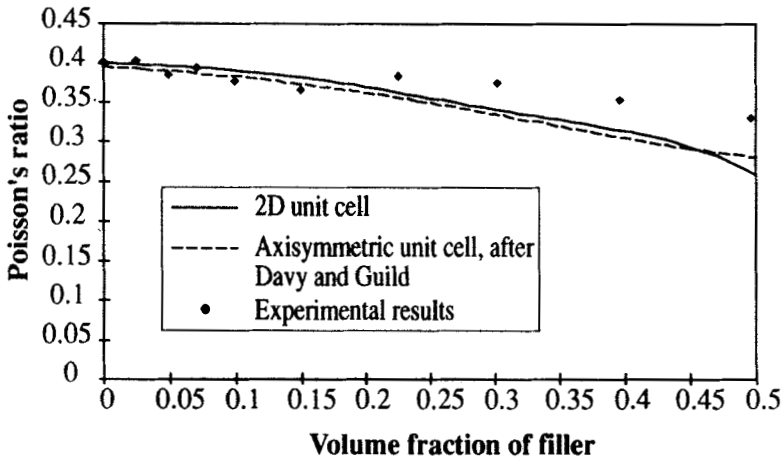

FIGURE 6 Poisson's ratio as a function of volume fraction for data set i), *i.e.* glass spheres in epoxy.

As the volume fraction increases, the three-dimensional model tends to overpredict the stiffness, whereas the two-dimensional model underpredicts it. For volume fractions around 50%, the three-dimensional model once again makes a good prediction for the actual material properties. The two-dimensional model at this point, however, is in error by about 30%. To understand why the predictions follow such a trend, the effect that the nature of the particle dispersion has on a unit cell must be considered.

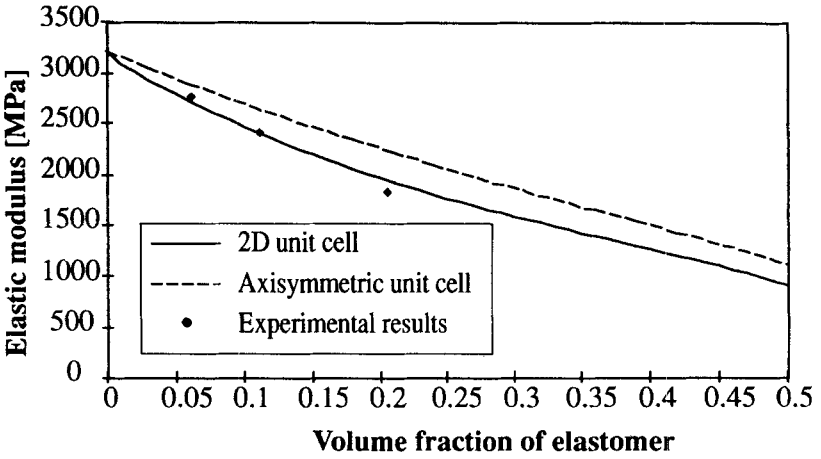

FIGURE 7 Elastic modulus as a function of volume fraction for data set ii), *i.e.* rubber spheres in epoxy. Finite element results for a two-dimensional unit cell and an axisymmetric unit cell.

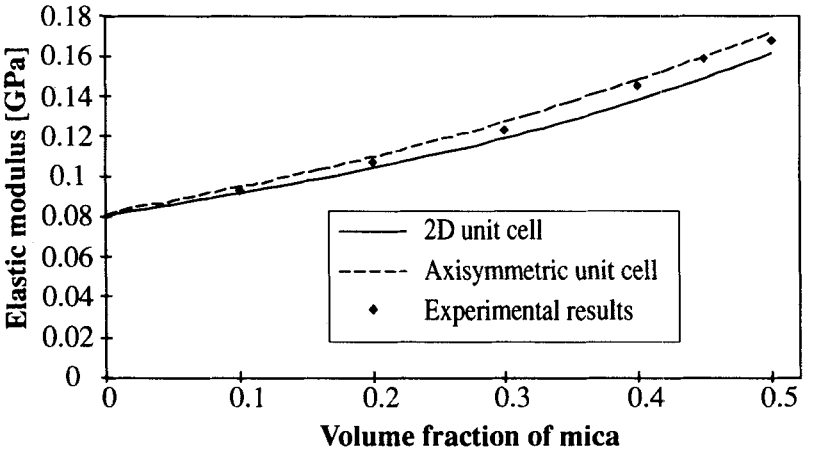

FIGURE 8 Elastic modulus as a function of volume fraction for data set iii), *i.e.* mica particles in glass. Finite element results for a two-dimensional unit cell and an axisymmetric unit cell.

The unit cell is chosen to have a mean interparticle distance identical to the expected interparticle distance encountered in the real system. The probability density function for interparticle distance is only symmetrical for points (as opposed to particles) distributed in three dimensions. For particles having a finite radius, or in two dimensions, the resulting Poisson distribution function of interparticle distance is asymmetrically distributed around this mean value, which has the effect of decreasing the contribution from regions of large interparticle distance (or large unit cells). This leads to an overestimation of the effect that the particles have on the system behaviour.

For high volume fractions, the dispersion approaches a uniform distribution, the variability decreases and the three-dimensional predicted properties once again approach the actual properties. The overprediction is most apparent at intermediate volume fractions since the change in stiffness is only small at low volume fractions.

Davy and Guild[29] modify the data using a dispersion factor. The dispersion factor arises because of two effects: the asymmetry of the probability density function for the interparticle distance and a second differential error term that relates the loading that individual cells experience to the loading of the whole material. In the axisymmetric analysis, the dispersion factor makes very little difference but, in a study of fibre composites, employing what is essentially a two-dimensional model, Guild, Hogg and Davy[37] found the dispersion factor to make a bigger difference over a longer range than is the case in three dimensions.

Both models predict that Poisson's ratio decreases with increasing volume fraction. The only difference is that the two-dimensional cell predicts a higher rate of decrease at volume fractions approaching 50%. The implication is that the filler particles inhibit the orthogonal Poisson behaviour. This seems entirely reasonable, even though the experimental results do not agree very well with either model at high volume fractions of filler. As far as the second and third data sets are concerned; the two-dimensional model actually seems to predict the behaviour of the rubber-filled epoxy best, although the data are limited, while both models give a reasonable prediction of the mica particles in glass. Although the filler and matrix moduli here are both an order of magnitude greater than the corresponding matrix and filler in the adhesive currently under investigation, the mica is in the form of irregular, angular particles that bear a marked resemblance to the adhesive filler. This indicates that the theory for spherical particles can be adapted to these random shapes.

5. MODELLING OF ADHESIVE BEHAVIOUR

5.1 Constitutive Adhesive Material Properties

The two-dimensional analysis can be used to model the adhesive investigated in the present study since the volume fraction of filler is relatively low. For the three data sets investigated in the previous section, the constitutive material properties were known. For the adhesive, only the composite properties are known with any accuracy[23]. The filler has a chemical composition similar to chalk, with a volume fraction around 12%. Howatson *et al.*[38] indicate that a Poisson's ratio of 0.2 and a tensile modulus in the range 10000 MPa to 17000 MPa would not be unreasonable for chalk. For the volume fraction involved, it has been found that changing the chalk modulus between these values only changes the composite modulus by about 5%, and Poisson's ratio by about 0.5%.

The epoxy matrix properties were established by performing a two-dimensional unit cell analysis for varying values of elastic modulus and Poisson's ratio until the calculated composite values matched the experimentally-derived values at a volume fraction of 12%. The assumed filler modulus and Poisson's ratio were, respectively, 10 GPa and 0.2. Table II summarises the results. The calculated and experimental

TABLE II
Summary of results from a unit cell analysis of the adhesive system, assuming the chalk to have modulus of 10000 MPa, Poisson's ratio of 0.2 and a volume fraction of 12%

	Assumed Matrix Value	Calculated Composite value	Experimental Composite value
E[MPa]	2892	3265	3265
v	0.425	0.4057	0.406

composite material properties agree to three significant figures and the assumed values for the matrix are comparable with similar systems (see Table I, set i)).

5.2 Modelling the Damage Structures

5.2.1 Introduction

SEM experiments show that the damage in the adhesive takes two forms: particle debonding and particle cracking. Each phenomenon results in non-linear behaviour. In hydrostatic compression, the material behaves as if undamaged but, under hydrostatic tension, both morphologies soften the adhesive. In the case where the array consists of horizontal cracks, the material behaves in an orthotropic way, and obeys the matrix equation:

$$\underline{\varepsilon} = \underline{\mathbf{D}}\,\underline{\sigma}$$

where:

$$\underline{\mathbf{D}} = \begin{bmatrix} 1/E_x & -v_{yx}/E_y & -v_{zx}/E_z & 0 & 0 & 0 \\ -v_{xy}/E_x & -1/E_y & -v_{zy}/E_z & 0 & 0 & 0 \\ -v_{xz}/E_x & -v_{yz}/E_y & 1/E_z & 0 & 0 & 0 \\ 0 & 0 & 0 & 1/G_{xz} & 0 & 0 \\ 0 & 0 & 0 & 0 & 1/G_{yz} & 0 \\ 0 & 0 & 0 & 0 & 0 & 1/G_{xy} \end{bmatrix}$$

The matrix $\underline{\mathbf{D}}$ is symmetric, and the nine independent material constants can be evaluated from three independent load cases. The unit cell can be modified easily to model an array of cracked particles, aligned cracks, holes, undamaged particles or debonded particles (see Figure 9). In the following sections, the effective material properties for different damaged morphologies are calculated using a two-dimensional unit cell and assuming linear elastic constitutive material behaviour.

5.2.2 Cracked Particles

A two-dimensional cell represents a cylinder of filler in a block of matrix, which is wholly orthotropic when a crack is introduced in the particle. This introduces the anomaly that although plane stress or plane strain may be assumed in the third dimension, in order to get correct macroscopic behaviour, material properties in all

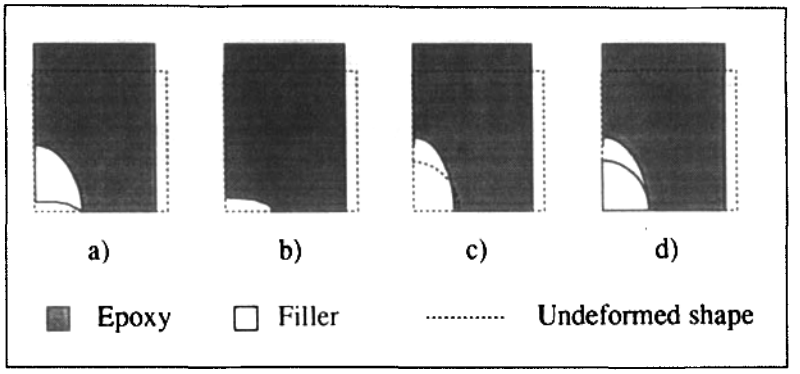

FIGURE 9 Deformed cell shapes to show how the unit cell can be modified to model: a) aligned, cracked particles; b) aligned cracks; c) holes; d) debonded particles.

three coordinate directions must be supplied to the finite element analysis package. Thus, effective material properties in the z-direction must be deduced. Ignoring the shear terms for the time being leaves six unknown constants to determine. Three independent load cases are, therefore, required to define the compliance matrix. Strain in the x- and y-directions can be applied using equations (1) to (2) and their extensions. Such loading will induce x- and y-direction stresses, and either a strain or stress in the z-direction, depending on whether the model is analysed under plane stress or plane strain conditions. The average stress the cell experiences in the x-direction is found by integrating the nodal x-direction stresses over a vertical boundary. The average y-direction stress is found in a similar way from integrating over a horizontal boundary. The products of individual z-direction elemental stresses (or strains) and element areas are summed and divided by the cell area in order to give a "weight-averaged" value for the stress (or strain) in the z-direction. Table III gives the results for three independent tensile loading regimes and a shear loading regime.

The linear terms in the D matrix can be calculated from Table III to be as follows:

$$\underline{\mathbf{D}} = \begin{bmatrix} 306.5 & -126.9 & -135.6 & 0 & 0 & 0 \\ -126.9 & 336.6 & -142.2 & 0 & 0 & 0 \\ -135.6 & -142.2 & 340.8 & 0 & 0 & 0 \\ 0 & 0 & 0 & 893.7 & 0 & 0 \\ 0 & 0 & 0 & 0 & 1/G_{yz} & 0 \\ 0 & 0 & 0 & 0 & 0 & 1/G_{xy} \end{bmatrix} \text{MPa}^{-1}$$

The weight averaged stresses and strains in Table III do not give wholly accurate results. Consequently, a D matrix calculated using them is not fully symmetric. The four terms in the upper left hand corner are unaffected since they do not rely on the z-direction stresses or strains, but the differences between the $-\nu_{xz}/E_z$ and $-\nu_{zx}/E_x$,

TABLE III
The four independent load cases for substitution into the compliance matrix for the unit cell containing cracked particles

Load Case	ε_x	ε_y	ε_z	σ_x [MPa]	σ_y [MPa]	σ_z [MPa]	τ_{xy} [MPa]	γ_{xy}
1	0.01	0	0.00707	38.7	14.6	0		
2	0	0.01	0.00673	14.6	35.2	0		
3	0	0.01	0	50.3	69.4	47.3		
4							11.19	0.01

and $-\nu_{yz}/E_z$ and $-\nu_{zy}/E_y$ terms is of the order of 5%. The appropriate terms have, therefore, been averaged to give the D matrix shown here. Only one shear term has been calculated, since the shear moduli related to the other two terms are not needed for a plane stress or plane strain analysis.

It is interesting to note that the $1/E_y$ and $1/E_z$ terms are close to each other, implying the cell is near to being transversely isotropic, even though there is no apparent reason why this should be the case. The elastic material constants that follow from this matrix are given in Table IV.

5.2.3 Particle Debonding

Debonded particles were modelled in plane strain using the same unit cell mesh as before (see Fig. 3), but contact elements are inserted between the particle and matrix. The unit cells were loaded by applying uniform strains in the x- and y-directions using the procedure outlined in section 4.2. Converged solutions were found only for the cases where the matrix remained in contact with the particle somewhere on its periphery. As soon as this condition is breached, the debonded particle becomes unconstrained, and the matrix can be considered to have a dispersion of holes. Figure 10 plots the variation of strain in the x-direction against the strain in the y-direction for 12% of filler. The regions in which the system behaves as if it contains holes and in which it behaves as if it contains fully-bonded particles are shown. The D matrix in each of these regions remains constant and isotropic. In the intermediate regions, the D matrix for the system is a function of the strain field and is orthotropic. In other words, both the x- and y-direction elastic moduli will differ depending on how much of the particle is in contact with the epoxy. The fully debonded/intermediate boundary can easily be found by considering the ratio of equatorial to polar strain of

TABLE IV
The elastic constants calculated using the fully compatible unit cell method

E_x [MPa]	E_y [MPa]	E_z [MPa]	G_{xy} [MPa]	ν_{yz}	ν_{xy}	ν_{xz}
3262	2971	2935	1119	0.422	0.4141	0.442

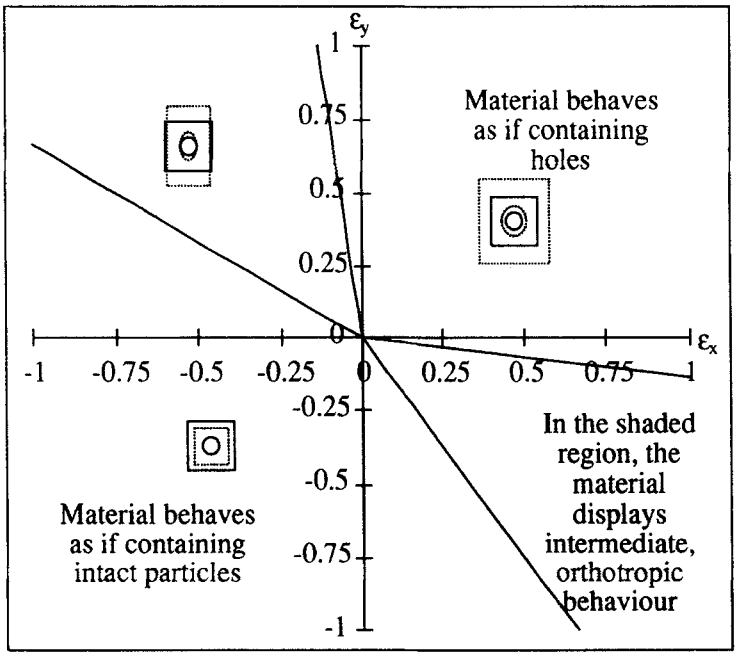

FIGURE 10 The various regions for debonded particle material behaviour in the adhesive system (particle volume fraction of 12%).

the hole in a unit cell. Figure 11 presents the results as a function of volume fraction.

Figure 12 and 13 show the results from the finite element investigation of debonded particles. The figures were derived by giving the unit cell a constant compressive strain

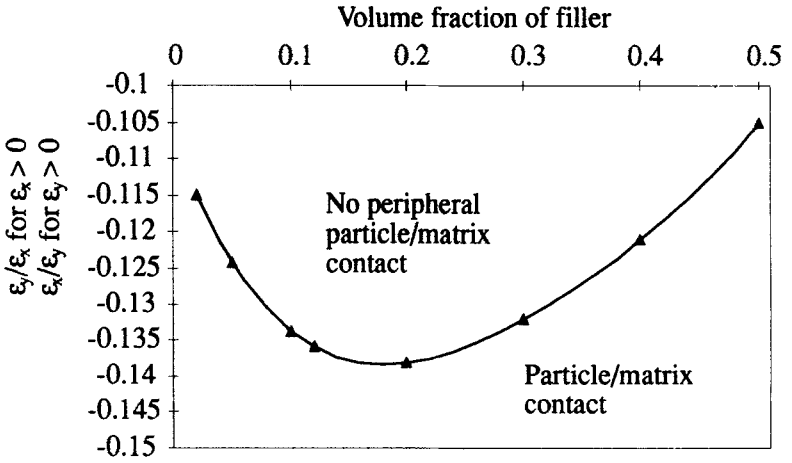

FIGURE 11 The ratio of the y to x strains necessary to cause debonded particles to behave as holes, presented as a function of volume fraction.

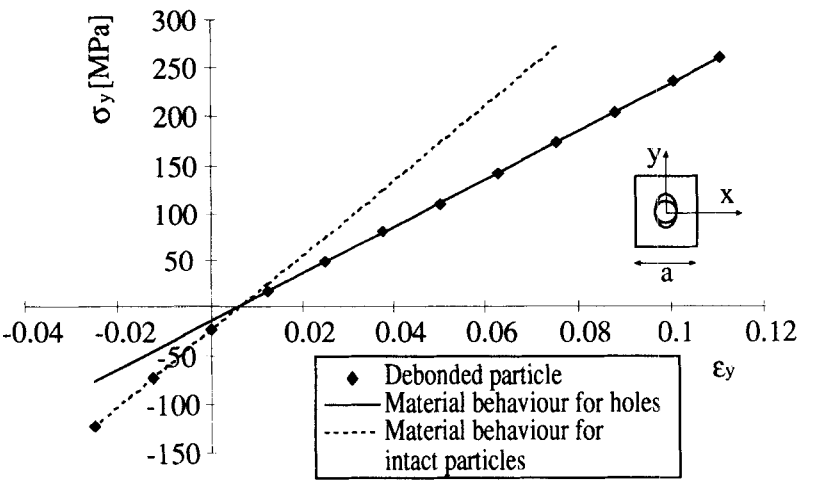

FIGURE 12 The y-direction stress/strain behaviour for epoxy containing partially-debonded particles. A compressive strain of 1.51% is applied in the x-direction so that the unit cell displays intermediate behaviour.

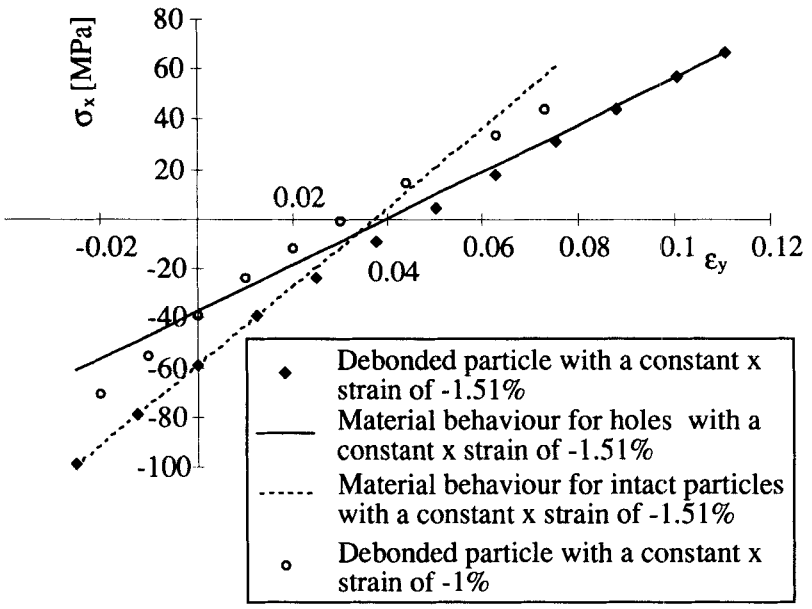

FIGURE 13 The x-direction stress as a function of y-strain behaviour for epoxy containing partially-debonded particles. A compressive strain is applied in the x-direction so that the unit cell displays intermediate behaviour. Increasing this strain shifts the material response to the right.

in the x-direction whilst applying a varying y strain so that the strain state remained within the shaded region of Figure 10. Figure 12 shows a stress/strain plot in the tensile (i.e., y) direction. When the stress (not the strain) is positive, the stress appears to follow the locus taken by material containing holes of the same size as the particles. When it is

negative, the stress behaviour approaches that of particles still wholly in contact. The stress in the tensile direction, then, appears to be unaffected by only partial debonding; it behaves either as if the particle is fully debonded or not at all debonded.

In contrast to this, the stress in the compressive (x) direction has a transition region as it changes from behaving like a hole into behaving like an undamaged particle. This can be seen in Figure 13 which plots the stress in the compressive (x) direction against the y strain. It also shows the effect of changing the constant compressive strain. As it is increased, the shape of the response is unchanged, and merely moves further to the right along the x-axis. The basic stress/strain equations in two dimensions for the debonded particle situation may be expressed:

$$\begin{bmatrix}\sigma_x\\ \sigma_y\end{bmatrix}=\begin{bmatrix}A(\varepsilon_x,\varepsilon_y) & B(\varepsilon_x,\varepsilon_y)\\ B(\varepsilon_x,\varepsilon_y) & C(\varepsilon_x,\varepsilon_y)\end{bmatrix}\begin{bmatrix}\varepsilon_x\\ \varepsilon_y\end{bmatrix}.$$

From Figure 12, it seems that σ_y is piece-wise linear. The values of B and C are given by the data for either holes or fully-bonded particles (see Table VI later), according to the strain state. Figure 13 demonstrates that σ_x is not linear, and it was decided to fit a second order polynomial to the data of form:

$$\sigma_x = a + b\varepsilon_x + c\varepsilon_y + d\varepsilon_x\varepsilon_y + e\varepsilon_x^2 + f\varepsilon_y^2. \tag{3}$$

Figure 14 plots the results and the values for the constants are given in Table V. The parameter a is close to zero compared with the other terms and, taking into account the very good fit, the data can be described by the equation:

$$\sigma_x = b\varepsilon_x + c\varepsilon_y + d\varepsilon_x\varepsilon_y + e\varepsilon_x^2 + f\varepsilon_y^2. \tag{4}$$

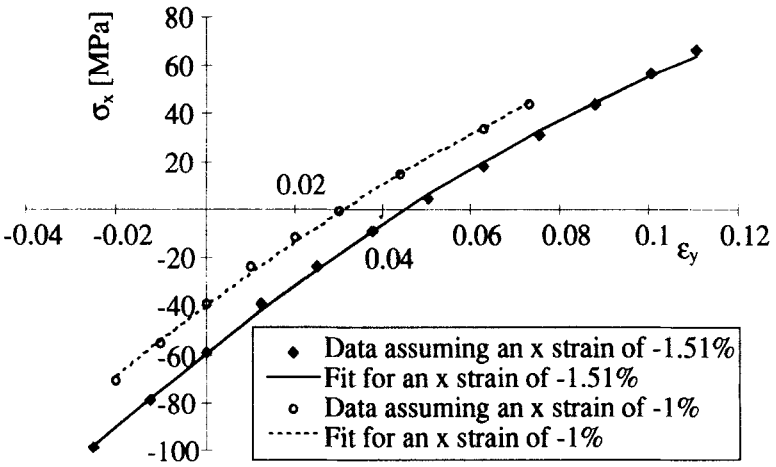

FIGURE 14 The variation of the stress, σ_x, with ε_y and its fit to Eq. (4) for two different strains in the x-direction.

TABLE V
The values of the constants a to f in equation 4

a	b	c	d	e	f
−0.4867	3937	1218	−15850	1792	−3076

The matrix equation can be rewritten:

$$\begin{bmatrix}\sigma_x\\ \sigma_y\end{bmatrix}=\begin{bmatrix}b+e\varepsilon_x+g\varepsilon_y & c+h\varepsilon_x+f\varepsilon_y\\ B & C\end{bmatrix}\begin{bmatrix}\varepsilon_x\\ \varepsilon_y\end{bmatrix} \tag{5}$$

where $g+h=d$ and are chosen so that the matrix remains symmetrical (g and h vary with strain). The above equation can be compared with:

$$\begin{bmatrix}\sigma_x\\ \sigma_y\end{bmatrix}=\frac{1}{1-\nu_{xy}\nu_{yx}}\begin{bmatrix}E_x & E_y\nu_{xy}\\ E_x\nu_{yx} & E_y\end{bmatrix}\begin{bmatrix}\varepsilon_x\\ \varepsilon_y\end{bmatrix} \tag{6}$$

which, knowing the constant values, allows the plotting of the material constants as functions of the strain state for a volume fraction of 12%, (Figs. 15 and 16). An important point to consider is the limits of applicability of Eq. (4). One limit where the matrix just loses contact with the particle equator has already been defined, and calculated as a function of volume fraction (Fig. 11). Figures 12 and 13 give a clue as to the other limit where debonding of the particle is just beginning. Figure 12 demonstrates that the stress in the y-direction is bilinear. As soon as the y-stress behaves as if

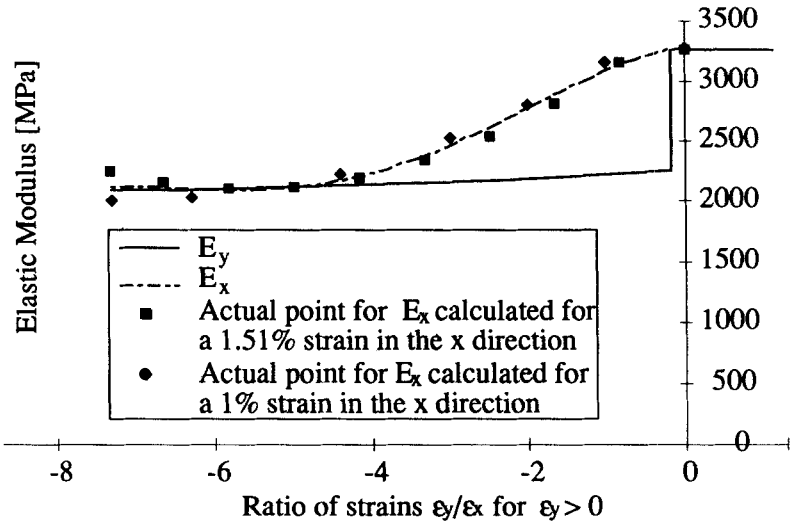

FIGURE 15 The variation of the orthogonal elastic moduli as a function of ε_y for constant ε_x, where x denotes the direction of the compressive strain required to keep the particles partially in contact with the matrix.

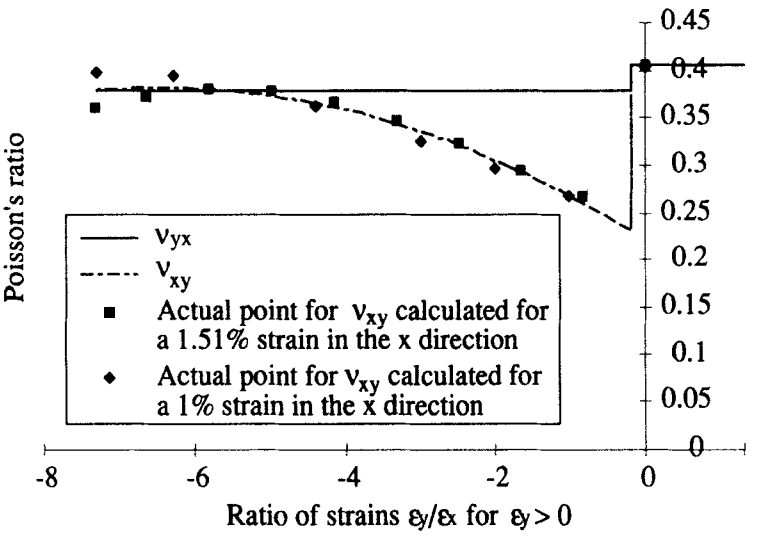

FIGURE 16 The variation of the orthogonal Poisson's ratios as a function of ε_y for constant ε_x, where x denotes the direction of the compressive strain required to keep the particles partially in contact with the matrix.

the material contained holes, then it is postulated that the material as a whole experiences intermediate behaviour. The strain at which this happens correlates with the strain at which Figure 13 deviates from the straight line asymptote and, physically speaking, is the point at which a void first appears at the pole of the particle. This point can be identified by equating the expressions for the y-stress in material containing fully-debonded and intact particles.

For holes:

$$\sigma_y = \frac{E_h \nu_h \varepsilon_x}{1-\nu_h^2} + \frac{E_h \varepsilon_y}{1-\nu_h^2}. \tag{7}$$

For intact particles

$$\sigma_y = \frac{E_i \nu_i \varepsilon_x}{1-\nu_i^2} + \frac{E_i \varepsilon_y}{1-\nu_i^2}. \tag{8}$$

From the unit cell analyses, it is known that the material properties for the two morphologies are as indicated in Table VI.

The changeover between fully bonded and intermediate material behaviour may be calculated by equating Eqs. (7) and (8), and substituting in the values in Table VI. It occurs when:

$$\varepsilon_y = -0.4516\varepsilon_x$$

Both these limits can be seen in Figures 15 and 16, which show E_x, E_y, ν_{yx} and ν_{xy} for varying ratios of horizontal to vertical strain. The graphs were calculated by construct-

TABLE VI
The calculated isotropic material properties for material containing a 12% volume fraction of holes and for a 12% volume fraction of intact particles

	Holes	Fully bonded particles
E(MPa)	2117	3265
ν	0.3795	0.406

ing the matrix Eq. (5), and comparing it with (6). E_y and ν_{yx} were given the appropriate values for holes or fully-bonded particles as laid out in Table VI, depending on which side of the fully-bonded/intermediate limit was the strain state. The curves for E_x and ν_{xy} are curve fits to the data obtained from the two different values of strain in the x-direction considered. The modulus in the x-direction decreases gradually to its final value at the intermediate/hole changeover and ν_{xy} rises steadily. The physical interpretation is that the appearance of a void at the particle pole causes the sudden change in all the material constants except E_x. This modulus is not so immediately sensitive to events occurring at the pole. As the amount of debonding increases, however, E_x and ν_{xy} tend to their limiting values for holes, which for a volume fraction of 12% is finally reached when $\varepsilon_x/\varepsilon_y = -7.35$ (Fig. 11), although Figures 15 and 16 would suggest that, for all practical purposes, no doubt due to very limited contact at the particle equator, a ratio of -5 is adequate.

6. CONCLUDING REMARKS

As far as experimentation is concerned, two things have been established: the volume fraction of filler, and the nature of crack propagation. Because of commercial sensitivity, it is not possible to reveal the exact nature of the adhesive, except that it consisted of an epoxy base, filled with 12.0% volume fraction of mineral particles between 0.5 μm. and 13 μm in diameter, and a median average diameter of 2.83 μm. Cracking was seen to originate at these particles, either by them debonding or cleaving through their bulk. The cracks thereafter coalesced to propagate the main crack.

It was chosen to model the damaged material using the unit cell, advocated by Davy and Guild. A two-dimensional square cell was used so that shear could be modelled. Although an axisymmetric cell, consisting of a sphere of filler in a cylinder of matrix, is a better representation, below 20% volume fraction the benefit is not great. In total, four different configurations were considered: fully-bonded particles, fully-debonded particles, cracked particles and partially-debonded particles. The first two configurations yielded constant but different isotropic material properties. The last two configurations yielded orthotropic material properties and, for the partially-debonded particles, the material properties are a function of strain state. Moreover, the type of damage affects the degree of softening. Debonded particles result in up to a 35% loss of stiffness, whereas cracked particles, even normal to the crack plane, only give a 9% reduction and, in the plane of the crack, there is virtually no difference. The Poisson effect is similarly reduced more for debonded particles than for cracked particles.

The preceding sections have shown how the finite element analysis of a unit cell may be used to predict elastic properties for material containing a certain morphological pattern, distributed randomly in three dimensions. In this case, the recurring pattern was particles intact or damaged by cracking or debonding, but the process may be equally well applied to other morphologies, for instance, rubber-toughened epoxy or fibre-reinforced polymer. In these last two examples, the technique has been used to investigate the stresses in the matrix induced by the presence of the second phase, but the effective damaged properties calculated here are for use in two distinct ways.

- A region in a specimen can be assigned appropriate degraded material properties based on a finite element analysis of the extent of damage. The redistribution of stress caused by the region can, therefore, be modelled, and the possible crack shielding effects analysed. Material failure parameters determined by explicitly modelling the damaged region, such as maximum stress, strain or critical strain energy release rate, will be more accurate than those determined assuming undamaged material.
- By simulating the progression of damage actually observed, damage initiation and propagation criteria can be generated. These can then be used to determine the growth of the damage zone, and hence the response of any joint made using this adhesive.

The worth of the approach is fully realised when the plastic response of the system is taken into account. From an analysis of the "best" and "worst" conditions (*i.e.*, a fully-debonded particle and a fully-intact particle), a comparison with the tensile stress/strain curve gives a probability density function of particle failure. This, of course, is a function of strain state and may be implemented in a finite element analysis, so that the amount of damage in terms of percentage of debonded filler at any particular point may be assessed.

From a knowledge of the failure loading for a particular adhesive joint configuration, a finite element model may be constructed, incorporating the appropriate level of damage in the macroscopic material properties. A unit cell can be given the critical loads extracted from this macro model so that failure criteria may be developed. This is the subject of current work and will be reported at a later stage.

Acknowledgements

The authors would like to thank the EPSRC for supporting this work through grant reference GR/H38683.

References

1. R. D. Adams and W. C. Wake, "*Structural Adhesive Joints in Engineering*" (Elsevier Applied Science Pub. 1984).
2. A. J. Kinloch, S. J. Shaw, D. A. Tod and D. L. Hunston, *Polymer*, **24**, 1341 (1983).
3. A. J. Kinloch, S. J. Shaw, D. A. Tod and D. L. Hunston, *Polymer*, **24**, 1355 (1983).
4. R. A. Pearson and A. F. Yee, *J. of Mater. Sci.*, **26**, 3828 (1991).
5. R. A. Pearson, A. K. Smith and A. F. Yee, *Proc. 2nd Int. Conf. on Deformation and Fracture of Composites* (Inst. of Matls., Manchester, 1993), p. 9.1.
6. A. Einstein, *Investigations on the Theory of Brownian Motion* (Dover, 1956), pp. 36–62.
7. R. Hill, *J. Mech. Phys. of Solids*, **11**, 357 (1963).

8. Z. Hashin, *Appl. Mechanics Reviews*, **17**, 1 (1964).
9. Z. Hashin, *Theory of Fiber Reinforced Materials*, NASA CR-1974 (1972).
10. B. D. Ripley, *Spatial Statistics* (John Wiley & Sons, 1981).
11. Z. Hashin, *J. Appl. Mech.*, **29**, 143 (1962).
12. Z. Hashin and S. Shtrikman, *J. Mech. Phys. Solids*, **11**, 127 (1963).
13. Z. Hashin, *Int. J. Solids and Structures*, **6**, 539 (1970).
14. Z. Hashin, *Int. J. Solids and Structures*, **6**, 979 (1970).
15. J. D. Eshelby, *Proc. Royal Society*, **A 241**, 376 (1957).
16. T. T. Wu, *Int. J. Solids and Structures*, **2**, 1 (1966).
17. B. Budianski, *J. Mech. Phys. Solids*, **13**, 223 (1965).
18. R. Hill, *J. Mech. Phys. Solids*, **13**, 213 (1965).
19. E. H. Kerner, *Proc. Phys. Soc.*, **B 69**, 807 (1956).
20. J. C. Smith, *J. Research of the Nat. Bureau of Standards*, **78A**, 355 (1974).
21. R. M. Christiansen and H. K. Lo, *J. Mech. Phys. Solids*, **27**, 315 (1979).
22. B. Budianski and R. J. O'Connell, *Int. J. Solids Structures*, **12**, 81 (1976).
23. A. Hoenig, *J. Solids Structures*, **15**, 137(1979).
24. N. Laws, G. D. Dvorak and M. Hejazi, *Mech. Mat.*, **2**, 123 (1983).
25. H. Horii and S. Nemat–Nasser, *J. Mech. Phys. Solids*, **31**, 155 (1983).
26. J. Aboudi and Y. Benveniste, *Eng. Frac. Mech.*, **26**, 171 (1987).
27. M. H. Santare, A. D. Crocombe and G. Anlas, *Eng. Fract. Mech.*, accepted for publication.
28. T. Gottesman, Z. Hashin and M. A. Brull, *Proc. ICCMS*, 749 (1980).
29. P. J. Davy and F. J. Guild, *Proc. R. Soc. Lond.*, **A 418**, 95 (1988).
30. M. B. D. Ellis, P. R. Andrews and J. S. Crompton, *Int. J. Adhesion and Adhesives*, **12** (2), 95 (1992).
31. G. Richardson, "Predicting Failure in Bonded Joints" Report 5, Ref. CDR608, University of Surrey (1994).
32. J. C. Smith, *J. Res. Nat. Bureau of Standards*, **80A**(1), 45 (1976).
33. R. A. Pearson and A. F. Yee, *J. Mater. Sci.*, **21**, 2462 (1986).
34. F. J. Guild and R. J. Young, *J. Mater. Sci.*, **24**, 2454 (1989).
35. D. P. A. Hasselmann and R. M. Fulrath, *J. Amer. Ceram. Soc.*, **48**, (4) 218 (1965).
36. B. D. Agarwal, G. A. Panizza and L. J. Broutman, *J. Amer. Ceram. Soc.*, **54** (12) 620 (1971).
37. F. J. Guild, P. J. Hogg and P. J. Davy, in *Proc. 4th Intl. Conf. on Fibre Reinforced Composites* (IMechE/PRI, Liverpool, 1990), C400/022, p. 89.
38. A. M. Howatson, P. G. Lund and J. D. Tod, *Engineering Tables and Data* (Chapman and Hall, London, 1972).
39. F. J. Guild and A. J. Kinloch, *J. Mater. Sci. Letters*, **13**, 629 (1994).